A Novel INS/USBL Integrated Navigation Scheme via Factor Graph Optimization

Liang Zhang, Li-Ta Hsu, *Member, IEEE*, and Tao Zhang

***Abstract*—Factor graph optimization (FGO) is a well-known approach in the robotics field. Due to multiple iterations and application of large amounts of data, it usually could superior performance than the Kalman Filter (KF) under complex scenarios. However, it is rarely used in the underwater environment, especially for applications based on fiber-optic inertial navigation. Taking the ultra-short baseline system (USBL) as the application background, a novel inertial navigation system (INS)/USBL integrated navigation scheme based on FGO is presented in this paper. The traditional pre-integration factor simplifies the earth rotation and coordinate system, which limits its application in high-precision sensors. This paper proposed an improved pre-integration model using the high precision measurements of fiber optics gyroscope in FGO. Simulation and field tests proved that, with the FGO method, improved accuracy of INS/USBL integration was obtained compared to the traditional KF method. It confirms the potential of FGO in the applications of underwater navigation and positioning.**

***Index Terms*—USBL, INS, graph optimization, integrated navigation, pre-integration model.**

I. Introduction

THE high precision navigation and positioning are of great importance for autonomous underwater vehicles (AUV) in the exploitation of marine resources, and target detection [1], [2]. Due to the low attenuation of underwater acoustic signals, an ultra-short baseline system (USBL) is a common navigation approach and can achieve high precision navigation and positioning in a certain area [3]. Besides, an inertial navigation system (INS) still plays an important role in underwater navigation due to its autonomy and short-term high precision characteristics [4], [5]. Thus, the INS/USBL integration attracts more attention in recent years.

The integration of the two navigation systems is critical to improving positioning accuracy. It is also one of the most important research directions of INS/USBL integration in recent years. The framework of INS/USBL integrated navigation can be divided into loosely-coupled (LC) and tightly-coupled (TC). Morgado first introduced the LC and TC INS/USBL integrated navigation scheme based on an extended Kalman filter (EKF) in 2006 [6] and verified it through field experiments [7]. But the INS mechanization is simplified, which means it is not suitable for high-precision strap-down INS. In 2016, a TC integrated navigation scheme based on high-precision INS modeling is proposed [8]. Then, considering the nonlinearity of the USBL measurement model, the cubature Kalman filter (CKF) [9] and Unscented Kalman Filter (UKF) [10] are applied to the INS/USBL integrated navigation system, which could avoid the linearization errors in KF. This is a relatively well-studied area. In recent years, many scholars focus on the localization problem in the presence of abnormal measurements of USBL. A Huber M-estimation-based filter is applied to the INS/USBL integrated navigation system in 2021 [11]. Subsequently, a maximum correntropy-based filter is also proposed by the same author [12], which played a better performance. From the point of view of noise modeling, Wang proposed a student's distribution-based robust filter applied to the LC [13] and TC [14] INS/USBL integration system, respectively. Thus, the research of integrated navigation algorithms can be summarized into three aspects:1) the LC or TC framework; 2) linearized or nonlinear filtering; 3) robust or adaptive filtering.

Almost all current studies on INS/USBL integration are based on filtering schemes. No matter how the filter is designed, it is difficult to further improve the positioning accuracy of the integrated navigation system. Thus, it is important to explore a new fusion approach for INS/USBL integration.

The optimization-based approach has been widely used in the field of robotics, such as vision [15] or light detection and ranging (LiDAR) [16] simultaneous localization and mapping (SLAM). The FGO approach is also expanding from the SLAM applications to other fields. FGO is firstly applied for global navigation satellite system (GNSS) positioning in 2012 [17]. Subsequently, FGO has had many successful applications in GNSS positioning [18], [19]. With the introduction of the pre-integration model [20], an inertial measurement unit (IMU) has been integrated into many navigation applications based on FGO. An in-vehicle sensors navigation with IMU using FGO is proposed [21]. The INS/GNSS integration is classic integrated navigation. The FGO approach has been successfully applied in INS/GNSS integration [22], [23]. Wen first compared the performances of FGO and KF algorithms in low-cost INS/GNSS

Manuscript received 18 March 2022; revised 22 April 2022; accepted 18 May 2022. Date of publication 26 May 2022; date of current version 19 September 2022. This work was supported in part by the Postdoc Matching Fund Scheme W22E, in part by the National Natural Science Foundation of China under Grant 52071080, in part by the Fundamental Research Funds for the Central Universities under Grant 2242021K1G008, and in part by the National Natural Science Foundation of Southeast University under Grant 9S20172204 through Remaining funds cultivation Project. The review of this article was coordinated by Prof. Sukumar PhD Kamalasadan. *(Corresponding author: Li-Ta Hsu.)*

Liang Zhang and Li-Ta Hsu are with the Department of Aeronautical and Aviation Engineering, Hong Kong Polytechnic University, Hong Kong (e-mail: zhangliang9203@163.com; lt.hsu@polyu.edu.hk).

Tao Zhang is with the School of Instrument Science and Engineering, Key Laboratory of Micro-Inertial Instrument and Advanced Navigation Technology, Ministry of Education, Southeast University, Nanjing 210096, China (e-mail: zhangtao22@seu.edu.cn).

Digital Object Identifier 10.1109/TVT.2022.3177739

0018-9545 © 2022 IEEE. Personal use is permitted, but republication/redistribution requires IEEE permission.
See https://www.ieee.org/publications/rights/index.html for more information.

Authorized licensed use limited to: Hong Kong Polytechnic University. Downloaded on July 13,2023 at 10:26:38 UTC from IEEE Xplore. Restrictions apply.

systems and confirmed that TC integration using FGO performs the best [24].

The FGO is proved to be superior to KF due to its multiple iterations and re-linearization. Thus, it has huge potential for underwater INS/USBL integration. However, the existing pre-integration model ignores the earth rotation and the coordinate system is inconsistent if using the absolute measurements. This also limits its application in underwater high precision INS.

The contributions of the paper are twofold:

1) Implementing FGO to INS/USBL integrated navigation system. Benefit from the multiple iterations and re-linearization of FGO, it will play superior performance to the KF in INS/USBL integration.
2) Considering earth rotation in the proposed IMU pre-integration model. The centripetal acceleration to the earth caused by the motion of the carrier and the Coriolis acceleration are both taken into consideration. Thus, the pre-integration model is more suitable for underwater applications with high-precision IMU. And the coordinate system between relative and absolute measurements is also unified.

The structure of the paper is as follows. The first section is the introduction and includes the current research status. The second section introduces the positioning principles of USBL and analyzes the main problem of the application of FGO. The third section introduces the new IMU pre-integration model. The fourth section introduces the FGO-based integrated navigation scheme. The fifth section verifies the effectiveness of the proposed FGO algorithm through simulation and field tests. The last section presents a summary.

II. Problem Statement

Before analyzing the integrated navigation system, several coordinate systems are defined first in Table I.

TABLE I
DEFINITION OF THE REFERENCE FRAMES IN THE PAPER

Reference frame	Definition
b-frame	Orthogonal reference frame aligned with IMU axes
n-frame	Navigation frame (n-frame). Orthogonal reference frame aligned with East–North–Up (E-N-U) geodetic axes.
u-frame	USBL frame.Orthogonal reference frame aligned with USBL axes.
i_{b0}-frame	Body inertial reference frame. It is formed by fixing the axes of the b-frame in the inertial space at the beginning of the navigation process
i_{n0}-frame	Navigation inertial reference frame. It is formed by fixing the axes of the n-frame in the inertial space at the beginning of the navigation process
g-frame	Geographic frame, in which the earth surface point is represented by latitude, longitude, and height.
w-frame	The world frame used in [15] is the i_{n0}-frame in this paper. (w-frame is still named in the paper for readability)

A. Introduction of Positioning Principles of USBL

The detailed positioning principles of USBL can be seen in [14]. The USBL consists of a transducer and a transponder placed on the bottom of the water.

The transducer transmits an acoustic signal to the transponder. The transponder returns the acoustic signal to the hydrophone then. By measuring the round trip time delay and the angle-of-arrival, the slant distance (r) and bearings (α, β) can be obtained as shown in Fig. 1.

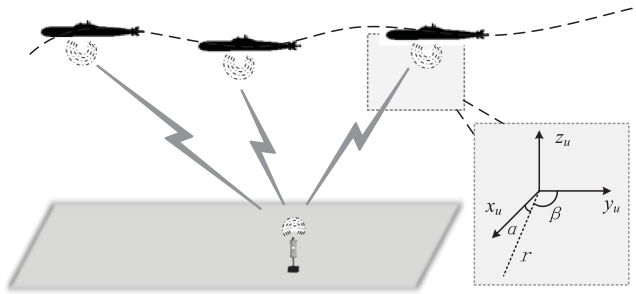

Fig. 1. Sketch of USBL positioning.

According to the USBL measurements, the transponder position in the u-frame ($\mathbf{t}^u$) can be expressed as

$$\mathbf{t}^u = \begin{bmatrix} t_{u,x} \\ t_{u,y} \\ t_{u,z} \end{bmatrix} = \begin{bmatrix} r\cos\alpha \\ r\cos\beta \\ -\sqrt{r^2 - t_{u,x}^2 - t_{u,y}^2} \end{bmatrix} \tag{1}$$

The absolute position of a transponder ($\mathbf{t}^g = [\,\lambda_t \; L_t \; h_t\,]^T$) and the transformation matrix ($\mathbf{C}_u^b$) between the u-frame and b-frame can be calibrated in advance [10]. λ denotes the latitude and L denotes the longitude. With the known attitude matrix $\mathbf{C}_b^n$ obtained by INS, the absolute position of AUV ($\mathbf{p}^g$) can be obtained.

$$\mathbf{p}^g = \mathbf{t}^g - \mathbf{R}_n^g \mathbf{C}_b^n \mathbf{C}_u^b \mathbf{t}^u \tag{2}$$

where $\mathbf{R}_n^g = \begin{bmatrix} 0 & \frac{1}{\mathrm{R_M+h}} & 0 \\ \frac{\mathrm{secL}}{(\mathrm{R_N+h})} & 0 & 0 \\ 0 & 0 & 1 \end{bmatrix}$, R_N, and R_M denote the principal radii of curvature along the prime-vertical normal and along the meridional sections, respectively. h denotes the height.

B. Problem of the Traditional IMU Pre-Integration Model

The propagation equation of INS in [15] is as follows.

$$\begin{cases} \mathbf{P}_{b_{k+1}}^w = \mathbf{P}_{b_k}^w + \mathbf{V}_{b_k}^w \Delta t_k + \int\int \left(\mathbf{R}_t^w \left(\hat{\mathbf{a}}_t - \mathbf{b}_{at} - \mathbf{n}_a\right) - \mathbf{g}^w\right) dt^2 \\ \mathbf{V}_{b_{k+1}}^w = \mathbf{V}_{b_k}^w + \int \left(\mathbf{R}_t^w \left(\hat{\mathbf{a}}_t - \mathbf{b}_{at} - \mathbf{n}_a\right) - \mathbf{g}^w\right) dt \\ \mathbf{q}_{b_{k+1}}^w = \mathbf{q}_{b_k}^w \otimes \int \frac{1}{2} \mathbf{\Omega} \left(\hat{\omega}_t - \mathbf{b}_{\omega t} - \mathbf{n}_\omega\right) dt \end{cases} \tag{3}$$

where $\mathbf{P}_{b_k}^w$ are the positions in w-frame at instant t_k. Similarly, $\mathbf{V}_{b_k}^w$ is the velocity. $\mathbf{q}_{b_k}^w$ are quaternions from b-frame

Authorized licensed use limited to: Hong Kong Polytechnic University. Downloaded on July 13,2023 at 10:26:38 UTC from IEEE Xplore. Restrictions apply.

to w-frame. $\mathbf{R}_t^w$ denotes the rotation matrix from b-frame to w-frame. $\hat{a}_t$ and $\hat{\omega}_t$are the outputs of the accelerometer and gyroscope. $\mathbf{b}_{at}$, $\mathbf{b}_{\omega t}$, $\mathbf{n}_a$, and $\mathbf{n}_\omega$ are parameters of the IMU noise model, which can be seen in [15]. $\mathbf{g}^w$ is the gravity in the w-frame. $\boldsymbol{\Omega}(\boldsymbol{\omega}) = \begin{bmatrix} -\lfloor\boldsymbol{\omega}\rfloor_\times & \boldsymbol{\omega} \\ -\boldsymbol{\omega}^T & \mathbf{0} \end{bmatrix}$.$\lfloor\boldsymbol{\omega}\rfloor_\times$ denotes the skew matrix.

Since the impact of earth rotation on IMU is ignored in (3), it is a simplified propagation equation. The integration error will be large if a high-precision IMU is adopted.

Besides, the w-frame in (3) is equivalent to the i_{n0}-frame. In underwater navigation, the n-frame is usually taken as the reference frame. The absolute position measurements are also in the n-frame. Thus, modifying the estimated state in i_{n0}-frame with the measurements in n-frame will make the estimation error large.

III. Improved IMU Pre-Integration Model

A. IMU Pre-Integration

The angular rates $\tilde{\omega}_{ib}^b$ and accelerations $\tilde{\mathbf{f}}^b$ output by IMU are modeled as follows.

$$\begin{aligned} \tilde{\omega}_{ib}^b &= \boldsymbol{\omega}_{ib}^b + \mathbf{b}_g + \mathbf{n}_g \\ \tilde{\mathbf{f}}^b &= \mathbf{f}^b + \mathbf{b}_a + \mathbf{n}_a \end{aligned} \tag{4}$$

where $\mathbf{b}_g$ and $\mathbf{b}_a$ denote the bias of the gyroscope and accelerometer. $\mathbf{n}_g$ and $\mathbf{n}_a$ denote the white noise, which is assumed as follows.

$$\begin{aligned} \mathbf{n}_g &\sim N\left(0, \sigma_g^2\right) \\ \mathbf{n}_a &\sim N\left(0, \sigma_a^2\right) \end{aligned} \tag{5}$$

We will derive a new pre-integration factor based on the strapdown inertial navigation propagation equation as follows.

$$\begin{cases} \dot{\mathbf{C}}_b^n = \mathbf{C}_b^n \left(\boldsymbol{\omega}_{nb}^b \times\right) \\ \dot{\mathbf{V}}^n = \mathbf{f}^n - \left(2\boldsymbol{\omega}_{ie}^n + \boldsymbol{\omega}_{\mathrm{en}}^{\mathrm{n}}\right) \times \mathbf{V}^n + \mathbf{g}^n \\ \dot{L} = \frac{V_N}{R_M + h} \\ \dot{\lambda} = \frac{secL}{R_N + h} V_E \\ \dot{h} = V_U \end{cases} \tag{6}$$

where $\mathbf{C}_b^n$ is the attitude rotation matrix. $\mathbf{V}^n = [V_E \ V_N \ V_U]^T$ is the velocity in the n-frame. $\mathbf{f}^n = \mathbf{C}_b^n(\tilde{\mathbf{f}}^b - \mathbf{b}_a)$, $\boldsymbol{\omega}_{nb}^b$ is expressed as follows.

$$\begin{aligned} \boldsymbol{\omega}_{nb}^b &= \boldsymbol{\omega}_{ib}^b - \mathbf{C}_n^b(\boldsymbol{\omega}_{ie}^n + \boldsymbol{\omega}_{en}^n) \\ \boldsymbol{\omega}_{ie}^n &= [0 \, \omega_{ie} \cos L \, \omega_{ie} \sin L]^T \\ \boldsymbol{\omega}_{en}^n &= [-V_N / (R_M + h) V_E / (R_N \\ &\quad + h) \, V_E \tan L / (R_N + h)]^T \end{aligned} \tag{7}$$

where $\boldsymbol{\omega}_{ie} = 7.2921151467\mathrm{e}^{-5}$ is the earth rotation rate.

First, the attitude pre-integration part will be analyzed.

According to (6), the attitude matrix can be expressed as follows [5].

$$\mathbf{C}_b^n = \mathbf{C}_{in0}^n \mathbf{C}_{ib0}^{in0} \mathbf{C}_b^{ib0} \tag{8}$$

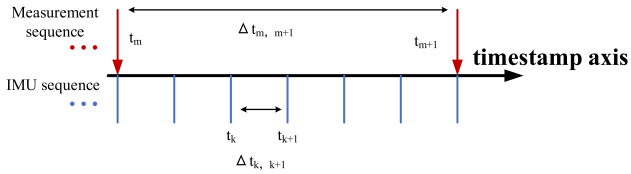

Fig. 2. Relationship of the timestamp used in the IMU preintegration t_m is the timestamp of the measurement and t_k is the timestamp of the IMU.

where $\mathbf{C}_{ib0}^{in0}$ is the initial attitude matrix. $\mathbf{C}_b^{ib0}$ and $\mathbf{C}_{in0}^n$ can be updated as follows.

$$\begin{aligned} \dot{\mathbf{C}}_b^{ib0} &= \mathbf{C}_b^{ib0} \left(\boldsymbol{\omega}_{ib}^b \times\right) \\ \dot{\mathbf{C}}_n^{in0} &= \mathbf{C}_n^{in0} \left(\boldsymbol{\omega}_{in}^n \times\right) \end{aligned} \tag{9}$$

where $\boldsymbol{\omega}_{in}^n = \boldsymbol{\omega}_{ie}^n + \boldsymbol{\omega}_{en}^n$.

The quaternion differential equation corresponding to $\mathbf{C}_b^{ib0}$ in (9) is as follows.

$$\dot{\mathbf{q}}_b^{b0} = \frac{1}{2} \boldsymbol{\Omega} \left(\boldsymbol{\omega}_{ib}^b - \mathbf{b}_g\right) \mathbf{q}_b^{b0} \tag{10}$$

Considering the coning error in the integration process, $\boldsymbol{\omega}_{ib}^b$ should be replaced by $\hat{\omega}_{ib}^b$ as follows.

$$\hat{\omega}_{ib}^b = \left(\Delta\boldsymbol{\theta}_k + \frac{1}{12} \Delta\boldsymbol{\theta}_{k-1} \times \Delta\boldsymbol{\theta}_k\right) / \Delta \mathrm{t} \tag{11}$$

where $\Delta\boldsymbol{\theta}_k = \boldsymbol{\omega}_{ib}^b \Delta \mathrm{t}$ denotes the angular increment at epoch *k*.

(8) can also be expressed through quaternion updating.

$$\mathbf{q}_b^n = \mathbf{q}_{in0}^n \otimes \mathbf{q}_{ib0}^{in0} \otimes \mathbf{q}_b^{ib0} \tag{12}$$

During the pre-integration interval $[t_m, t_{m+1}]$, the attitude from t_m to t_k $(k \in (m, m+1))$ can be expressed as follows.

$$\mathbf{q}_{bk}^{nk} = \mathbf{q}_{nm}^{nk} \otimes \mathbf{q}_{bm}^{nm} \otimes \mathbf{q}_{bk}^{bm} \tag{13}$$

The relationship between pre-integration intervals and IMU samples is shown in Fig. 2.

Thus, the attitude pre-integration between two measurements from t_m to t_{m+1} can be expressed as

$$\boldsymbol{\gamma}_{bm+1}^{bm} = \left(\left(\mathbf{q}_{bm+1}^{nm+1}\right)^{-1} \otimes \mathbf{q}_{nm}^{nm+1} \otimes \mathbf{q}_{bm}^{nm}\right)^{-1} \tag{14}$$

And $\boldsymbol{\gamma}_{bm+1}^{bm}$ can be calculated by (10) with the $\mathbf{q}_b^{b0}$ initialized as $[10, 00]^T$.

Second, the velocity pre-integration part will be analyzed.

According to (6), the velocity integration from t_m to t_{m+1} can be expressed as

$$\begin{aligned} \mathbf{V}_{m+1}^n = \mathbf{V}_m^n &+ \int_{t_m}^{t_{m+1}} \mathbf{C}_{nm}^{nt} \mathbf{C}_{bm}^{nm} \mathbf{C}_{bt}^{bm} \left(\tilde{\mathbf{f}}^b - \mathbf{b}_a\right) dt \\ &+ \int_{t_m}^{t_{m+1}} \left(\mathbf{g}^n - \left(2\boldsymbol{\omega}_{ie}^n + \boldsymbol{\omega}_{en}^n\right) \times \mathbf{V}^n\right) dt \end{aligned} \tag{15}$$

$\boldsymbol{\omega}_{ie}^n$ and $\boldsymbol{\omega}_{en}^n$ are associated with $\mathbf{V}_m^n$ and $\mathbf{P}_m^g$ but changes in velocity and position have very little effect on it as (7) shows. Usually, it is around 0.001 or 0.0001 orders of magnitude. The impact of velocity and position on $2\boldsymbol{\omega}_{ie}^n + \boldsymbol{\omega}_{en}^n$ will be studied in

Authorized licensed use limited to: Hong Kong Polytechnic University. Downloaded on July 13,2023 at 10:26:38 UTC from IEEE Xplore. Restrictions apply.

the future to accommodate a higher accuracy IMU. But, assume $2\boldsymbol{\omega}_{ie}^{n}+\boldsymbol{\omega}_{en}^{n}$ as a constant vector during a short period in this paper. The third term of the right side of (15) can be computed as follows.

$$\Delta\mathbf{V}_{cor/g(m)}^{n}=\mathbf{g}^{n}\Delta t_{m,m+1}-\left(2\boldsymbol{\omega}_{ie}^{n}+\boldsymbol{\omega}_{en}^{n}\right)\times\left(\mathbf{V}_{m+1}^{n}+\mathbf{V}_{m}^{n}\right)\frac{1}{2}\Delta t_{m,m+1}\tag{16}$$

Thus, the velocity pre-integration from t_m to t_{m+1} can be expressed as.

$$\boldsymbol{\beta}_{bm+1}^{bm}=\mathbf{C}_{nm+1}^{bm}\left(\mathbf{V}_{m+1}^{n}-\mathbf{V}_{m}^{n}-\mathbf{g}^{n}\Delta t_{m,m+1}+\left(2\boldsymbol{\omega}_{ie}^{n}+\boldsymbol{\omega}_{en}^{n}\right)\times\left(\mathbf{V}_{m+1}^{n}+\mathbf{V}_{m}^{n}\right)\frac{1}{2}\Delta t_{m,m+1}\right)\tag{17}$$

$\boldsymbol{\beta}_{bm+1}^{bm}$ can be calculated with the IMU measurements by the following.

$$\boldsymbol{\beta}_{bm+1}^{bm}=\int_{t_m}^{t_{m+1}}\mathbf{C}_{bt}^{bm}\left(\tilde{\mathbf{f}}^{b}-\mathbf{b}_{a}\right)dt\tag{18}$$

Then, the position pre-integration part will be analyzed.

According to (6), the position integration from t_m to t_{m+1} can be expressed as

$$\mathbf{P}_{m+1}^{n}=\mathbf{P}_{m}^{n}+\mathbf{V}_{m}^{n}\Delta t_{m,m+1}+\mathbf{C}_{bm}^{nm+1}\boldsymbol{\alpha}_{bm+1}^{bm}+\frac{1}{2}\mathbf{g}^{n}\Delta t_{m,m+1}^{2}-\frac{1}{2}\left(2\boldsymbol{\omega}_{ie}^{n}+\boldsymbol{\omega}_{en}^{n}\right)\times\mathbf{V}_{m}^{n}\Delta t_{m,m+1}^{2}\tag{19}$$

Thus, the position pre-integration from t_m to t_{m+1} can be expressed as

$$\boldsymbol{\alpha}_{bm+1}^{bm}=\mathbf{C}_{nm+1}^{bm}\left(\mathbf{P}_{m+1}^{n}-\mathbf{P}_{m}^{n}-\mathbf{V}_{m}^{n}\Delta t_{m,m+1}-\frac{1}{2}\mathbf{g}^{n}\Delta t_{m,m+1}^{2}+\frac{1}{2}\left(2\boldsymbol{\omega}_{ie}^{n}+\boldsymbol{\omega}_{en}^{n}\right)\times\mathbf{V}_{m}^{n}\Delta t_{m,m+1}^{2}\right)\tag{20}$$

$\boldsymbol{\alpha}_{bm+1}^{bm}$ can be calculated with the IMU measurements by the following.

$$\boldsymbol{\alpha}_{bm+1}^{bm}=\iint_{t_m}^{t_{m+1}}\mathbf{C}_{bt}^{bm}\left(\tilde{\mathbf{f}}^{b}-\mathbf{b}_{a}\right)dt\tag{21}$$

Note that $\mathbf{P}_{m+1}^{n}$ is a relative position in the n-frame. To obtain the absolute position in the g-frame, $\mathbf{P}_{m+1}^{n}$ should be transformed to $\mathbf{P}_{m+1}^{g}$ with the initial absolute position $\mathbf{P}_{0}^{g}$ as follows.

$$\mathbf{P}_{m+1}^{g}=\mathbf{P}_{0}^{g}+\mathbf{R}_{n}^{g}\mathbf{P}_{m+1}^{n}\tag{22}$$

$\mathbf{P}_{m+1}^{g}$ is used to update the earth rotation parameters such as $\boldsymbol{\omega}_{in}^{n}$ and $\boldsymbol{\omega}_{en}^{n}$ during the integration process.

B. Noise Propagation

The error state is defined as.

$$\delta\mathbf{z}_{t}=\left[\delta\boldsymbol{\alpha}_{bm+1}^{bm}\ \delta\boldsymbol{\beta}_{bm+1}^{bm}\ \delta\boldsymbol{\gamma}_{bm+1}^{bm}\ \delta\mathbf{b}_{g}\ \delta\mathbf{b}_{a}\right]^{\boldsymbol{T}}\tag{23}$$

Then, the state transition of the error term can be represented as follows.

$$\delta\dot{\mathbf{z}}_{t}=\mathbf{F}_{t}\delta\mathbf{z}_{t}+\mathbf{G}_{\boldsymbol{t}}\mathbf{n}_{\boldsymbol{t}}\tag{24}$$

where

$$\mathbf{F}_{\boldsymbol{t}}=\begin{bmatrix}\mathbf{0}&\mathbf{I}&\mathbf{0}&\mathbf{0}&\mathbf{0}\\ \mathbf{0}&\mathbf{0}&-\tilde{\mathbf{C}}_{bt}^{bm}\left(\tilde{\mathbf{f}}^{b}-\mathbf{b}_{a}\right)\times&\mathbf{0}&\tilde{\mathbf{C}}_{bt}^{bm}\\ \mathbf{0}&\mathbf{0}&-\left(\tilde{\omega}_{ib}^{b}-\mathbf{b}_{g}\right)\times&-\mathbf{I}&\mathbf{0}\\ \mathbf{0}&\mathbf{0}&\mathbf{0}&\mathbf{0}&\mathbf{0}\\ \mathbf{0}&\mathbf{0}&\mathbf{0}&\mathbf{0}&\mathbf{0}\end{bmatrix}$$

$$\mathbf{G}_{\boldsymbol{t}}=\begin{bmatrix}\mathbf{0}&\mathbf{0}\\ \mathbf{0}&\tilde{\mathbf{C}}_{bt}^{bm}\\ -\mathbf{I}&\mathbf{0}\\ \mathbf{0}&\mathbf{0}\\ \mathbf{0}&\mathbf{0}\end{bmatrix},\mathbf{n}_{\boldsymbol{t}}=\begin{bmatrix}\mathbf{n}_{g}\\ \mathbf{n}_{a}\end{bmatrix}\tag{25}$$

Thus, the pre-integration covariance matrix Σ_{bt}^{imu} can be propagated as follows.

$$\Sigma_{bt}^{imu}=\boldsymbol{\Phi}_{t}\Sigma_{bt-1}^{imu}\boldsymbol{\Phi}_{t}^{T}+\int_{t-1}^{t}\boldsymbol{\Phi}_{\boldsymbol{t}}\mathbf{G}_{\boldsymbol{t}}\mathbf{Q}\mathbf{G}_{t}^{T}\boldsymbol{\Phi}_{t}^{T}dt\tag{26}$$

where $\Sigma_{bm}^{imu}=0\quad(t=m)$, $\boldsymbol{\Phi}_{t}\approx\mathbf{I}+\mathbf{F}_{\boldsymbol{t}}\Delta t$, $\mathbf{Q}=\mathrm{diag}[\sigma_{g}^{2},\sigma_{a}^{2}]$.

The Jacobian matrix can be propagated as follows.

$$\mathbf{J}_{\boldsymbol{m},\boldsymbol{t}}=\boldsymbol{\Phi}_{\boldsymbol{t}}\mathbf{J}_{m,t-1}\tag{27}$$

where $\mathbf{J}_{m,m}$ is initialized as an identity matrix.

According to the Jacobian matrix and covariance matrix, the pre-integration measurements with respect to bias can be computed as follows [15].

$$\begin{cases}\tilde{\boldsymbol{\alpha}}_{bm+1}^{bm}\approx\boldsymbol{\alpha}_{bm+1}^{bm}+\mathbf{J}_{bg}^{\alpha}\delta\boldsymbol{b}_{g}+\mathbf{J}_{ba}^{\alpha}\delta\mathbf{b}_{a}\\ \tilde{\boldsymbol{\beta}}_{bm+1}^{bm}\approx\boldsymbol{\beta}_{bm+1}^{bm}+\mathbf{J}_{bg}^{\beta}\delta\boldsymbol{b}_{g}+\mathbf{J}_{ba}^{\beta}\delta\boldsymbol{b}_{a}\\ \tilde{\boldsymbol{\gamma}}_{bm+1}^{bm}\approx\boldsymbol{\gamma}_{bm+1}^{bm}\otimes\begin{bmatrix}1\\ \frac{1}{2}\mathbf{J}_{bg}^{\gamma}\delta\mathbf{b}_{g}\end{bmatrix}\end{cases}\tag{28}$$

where $\mathbf{J}_{bg}^{\alpha}$ is the sub-matrix of $\mathbf{J}_{\boldsymbol{m},\boldsymbol{m+1}}$ whose location is corresponding to $\frac{\delta\boldsymbol{\alpha}_{bm+1}^{bm}}{\delta\mathbf{b}_{g}}$. The same definition is used for $\mathbf{J}_{ba}^{\alpha}$, $\mathbf{J}_{bg}^{\beta}$, $\mathbf{J}_{ba}^{\beta}$, and $\mathbf{J}_{bg}^{\gamma}$.

IV. FGO Based INS/USBL Integrated Navigation Scheme

The integrated navigation problem is a typical maximum likelihood estimation (MAP) problem. Thus, the INS/USBL integration can be formulated as the following.

$$\tilde{\mathbf{x}}=\mathrm{argmax}\prod_{k,i}P\left(\mathbf{z}_{k,i}|\mathbf{x}_{k}\right)\prod_{k}P\left(\mathbf{x}_{k}|\mathbf{x}_{k-1}\right)\tag{29}$$

Authorized licensed use limited to: Hong Kong Polytechnic University. Downloaded on July 13,2023 at 10:26:38 UTC from IEEE Xplore. Restrictions apply.

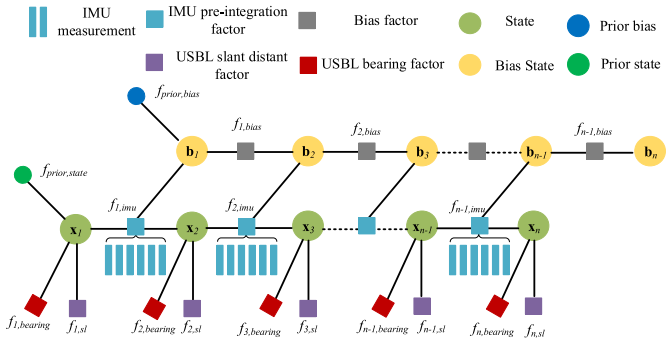

Fig. 3. Graph model of the proposed INS/USBL integration.

where $\mathbf{z}_{k,i}$ denotes the USBL measurements at epoch *k*. $\mathbf{x}_k$ denotes the system state at *k*. *S*ymbol *i* denotes the *i-th* measurement at epoch *k*. $\tilde{\mathbf{x}}$ is the optimal state estimation.

In FGO, the optimal estimate can be obtained by all the measurement factors. The MAP problem can be expressed as follows.

$$\tilde{\mathbf{X}} = \underset{x}{\operatorname{argmax}} \left(\prod_j f_j\left(\mathbf{x}_j\right) \right)$$
$$f_j\left(\mathbf{x}_j\right) \propto \exp\left(-\left\| h_j\left(\mathbf{x}_j\right) - \mathbf{z}_j \right\|^2_{\Sigma_j} \right) \tag{30}$$

where $f_j(\mathbf{x}_j)$ is the *j-th* factor. $h_j(\cdot)$ denotes the observation function associated with the *j-th* measurement $\mathbf{z}_j$. $\mathbf{X} = \{\mathbf{x}_1, \mathbf{x}_2, \ldots, \mathbf{x}_k, \ldots\}$ denotes the states that need to be estimated. Σ_j is the covariance matrix.

(30) can be reformulated as follows [25].

$$\tilde{\mathbf{X}} = \underset{\mathbf{x}}{\operatorname{argmax}} \left(\sum_j \left\| h_j\left(\mathbf{x}_j\right) - \mathbf{z}_j \right\|^2_{\Sigma_j} \right) \tag{31}$$

where $j \in [0, n]$, *n* is the sliding-window size.

Thus, the FGO problem can be formulated as a nonlinear least-squares problem as (31) shows. FGO can take full advantage of the historical information. However, the KF method recursively estimates the current state based on the previous state and the observation measurements at the current epoch. The FGO structure of the INS/USBL is shown in Fig. 3.

The state vector is defined as follows.

$$\mathbf{X} = \left[\mathbf{x}_0, \mathbf{x}_1, \mathbf{x}_2, \ldots \mathbf{x}_n\right]^T$$
$$\mathbf{x}_k = \left[\mathbf{P}^n_k, \mathbf{V}^n_k, \mathbf{q}^{nk}_{bk}, \mathbf{b}_{ak}, \mathbf{b}_{gk}\right]^T k \in [0, n] \tag{32}$$

where $\mathbf{X}$ is the state set. The position, velocity, attitude, and bias are treated as the state vector in the FGO.

The error factors described in Fig. 3 will be introduced in detail next.

A. The IMU Pre-Integration Factor

According to the pre-integration measurements in (14), (17), (20,) and (28), the residuals of IMU pre-integration can be computed as follows.

$$r_{imu}\left(\mathbf{z}^{bm}_{bm+1}, \mathbf{X}\right) = \begin{bmatrix} \boldsymbol{\alpha}^{bm}_{bm+1} - \tilde{\boldsymbol{\alpha}}^{bm}_{bm+1} \\ \boldsymbol{\beta}^{bm}_{bm+1} - \tilde{\boldsymbol{\beta}}^{bm}_{bm+1} \\ 2\left[\left(\mathbf{q}^{nm+1}_{bm+1}\right)^{-1} \otimes \mathbf{q}^{nm+1}_{nm} \otimes \mathbf{q}^{nm}_{bm} \otimes \tilde{\boldsymbol{\gamma}}^{bm}_{bm+1}\right]_{xyz} \\ \mathbf{b}_{gm+1} - \mathbf{b}_{gm} \\ \mathbf{b}_{am+1} - \mathbf{b}_{am} \end{bmatrix} \tag{33}$$

where $2[\cdot]_{xyz}$ is used to extract the rotation vector of a quaternion.

B. USBL Slant Distant Factor

First, the absolute position $\mathbf{t}^g$ should be transformed to a relative position in the n-frame with the initial position $\mathbf{P}^g_0$. The transponder position $(\mathbf{t}^n)$ can be expressed as follows.

$$\mathbf{t}^n = \left(\mathbf{R}^g_n\right)^{-1}\left(\mathbf{t}^g - \mathbf{P}^g_0\right) \tag{34}$$

The slant distance can be expressed as follows.

$$r = \left\| \mathbf{t}^n - \mathbf{P}^n \right\| \tag{35}$$

Thus, the residual of the slant distance factor can be computed as follows.

$$\boldsymbol{r}_{sl}\left(\mathbf{Z}_{sl,m}, \mathbf{X}\right) = \left\| \mathbf{t}^n - \mathbf{P}^n \right\| - r \tag{36}$$

C. USBL Bearing Factor

According to (2) and (34), the relative transponder position in the b-frame can be expressed as follows.

$$\mathbf{t}^u = \mathbf{C}^u_b \mathbf{C}^b_n \left(\mathbf{t}^n - \mathbf{P}^n\right) \tag{37}$$

According to (1), the bearings α and β can be computed in the u-frame as follows.

$$\begin{cases} \alpha &= acos\left(t_{u,x}/r\right) \\ \beta &= acos\left(t_{u,y}/r\right) \end{cases} \tag{38}$$

Thus, the residuals of the bearing factors can be computed as follows.

$$\boldsymbol{r}_{br}\left(\mathbf{Z}_{br,m}, \mathbf{X}\right) = \begin{bmatrix} \operatorname{acos}\left(t_{u,x}/r\right) - \alpha \\ \operatorname{acos}\left(t_{u,y}/r\right) - \beta \end{bmatrix} \tag{39}$$

Based on the above measurement residuals, the following MAP estimation equation can be obtained.

$$\min_x \left\{ \left\| \mathbf{r}_p - \mathbf{H}_p \mathbf{X} \right\|^2_{\Sigma_p} + \sum_{m \in [0,n]} \left\| r_{imu}\left(\mathbf{z}^{bm}_{bm+1}, \mathbf{X}\right) \right\|^2_{\Sigma^{imu}_{bm+1}} + \sum_{m[0,n]} \left\| \mathbf{r}_{sl}\left(\mathbf{Z}_{sl,m}, \mathbf{X}\right) \right\|^2_{\Sigma_{sl,m}} + \sum_{m \in [0,n]} \left\| \mathbf{r}_{br}\left(\mathbf{Z}_{br,m}, \mathbf{X}\right) \right\|^2_{\Sigma_{br,m}} \right\} \tag{40}$$

where $\left\| \mathbf{r}_p - \mathbf{H}_p \mathbf{X} \right\|^2_{\Sigma_p}$ denotes the prior information from marginalization and Σ_p is the prior covariance. $\Sigma_{sl,m}$ is the

Authorized licensed use limited to: Hong Kong Polytechnic University. Downloaded on July 13,2023 at 10:26:38 UTC from IEEE Xplore. Restrictions apply.

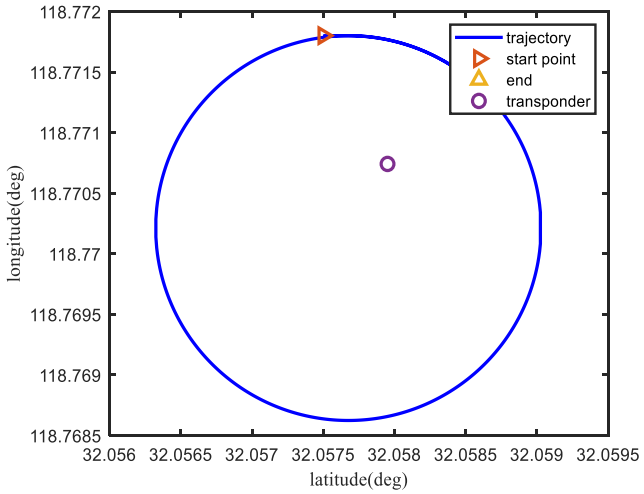

Fig. 4. Simulation trajectory.

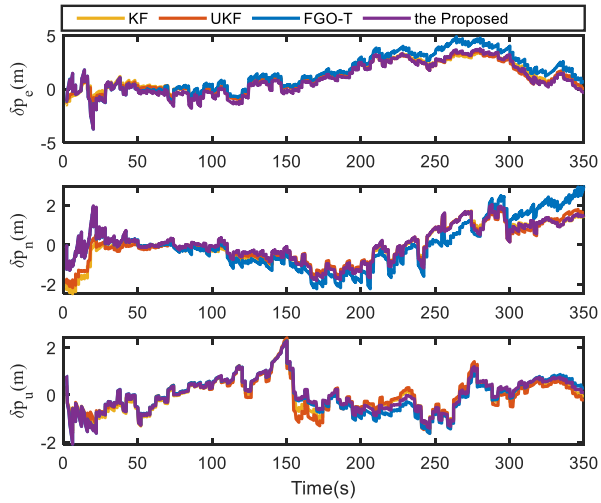

Fig. 5. Comparison of the position estimation error using the MEMS IMU.

measurement covariance of *m-th* slant distance, and $\Sigma_{br,m}$ is the measurement covariance of *m-th* bearing angles. $\Sigma_{sl,m}$ and $\Sigma_{br,m}$ are set according to the performance of the USBL. The Ceres Solver [26] is used to solve the MAP problem.

V. Simulation and Field Test Analysis

A. Simulation Test

To verify the effectiveness of the proposed algorithm, simulations are performed in this section.

Since the LC model usually shows worse performance compared to that of the TC model, only the TC INS/USBL integrated navigation model is compared in the paper.

Different types of filters can be used for multi-sensor integrated navigation, such as the adaptive and robust filter used for INS/GPS integration [27], [28], the federal filter used for the systems with more than two sensors [29]. The uncertainty of the measurement noise model is not considered in FGO. To make the validation method consistent, a standard Kalman filter and a nonlinear filter are selected for comparison. An FGO method considering the particularity of measurement noise will be carried out in future studies.

Symbols used for the simulations are as follows:

1) KF: the state-of-the-art error state Kalman filter based INS/USBL integrated navigation algorithm [8].
2) UKF: the unscented Kalman filter based INS/USBL integrated navigation algorithm.
3) FGO-T: the INS/USBL integrated navigation algorithm using the FGO with the traditional IMU pre-integration model described in [15].
4) the Proposed: the INS/USBL integrated navigation algorithm using the FGO with the proposed IMU pre-integration model described in Section III.

The window size in FGO-T and FGO is 50 s. The covariance matrix set in the three methods is the same.

The vehicle velocity is set as 3 m/s. The trajectory of the vehicle in the simulation experiment is shown in Fig. 4.

In the simulation, the sensor error parameters are set below. Two-level of IMU are set in the simulation. One is the fiber optics gyroscope (FOG) and the other is the micro-electro-mechanical systems (MEMS) IMU. The parameters of MEMS IMU are set according to an industrial-grade IMU module [30]. The parameters of FOG IMU and the USBL are referenced to actual instruments. The simulated IMU and USBL have been successfully used in our previous work [31].

a) FOG IMU

Gyro: bias $0.02^\circ/h$, random walk $0.01^\circ/\sqrt{h}$;

Accelerometer: bias 100 μg, random walk $100\,ug/\sqrt{Hz}$;

Output frequency: 200 Hz.

b) MEMS IMU

Gyro: bias standard deviation $15^\circ/h$, random walk $0.2^\circ/\sqrt{h}$;

Accelerometer: bias standard deviation 150mg, random walk $0.2\,m/s/\sqrt{h}$;

Output frequency: 200 Hz.

c) USBL

Bearing error: 0.2°; Slant distance error: 1.5m;

Output frequency: 1/2 Hz.

The initial position error: $\delta\boldsymbol{p}^n = [1\ 1\ 3]^{\mathrm{T}}\mathrm{m}$. The initial attitude error: $\delta\boldsymbol{\varphi}^n = [0.05^\circ\ 0.05^\circ\ 0.1^\circ]^{\mathrm{T}}$. The initial velocity error: $\delta\boldsymbol{v}^n = [0.1\ 0.1\ 0.1]^{\mathrm{T}}\mathrm{m/s}$. The initial position of the vehicle is $[118.7718^\circ E\ 32.0575^\circ N\ 18\mathrm{m}]^{\mathrm{T}}$. As underwater experiments are not possible at present, the movement on the water surface is simulated in this section. So the height of the vehicle position is positive.

According to the sensor error parameters of USBL, the covariance of USBL in FGO is set as $\Sigma_{sl,m} = 2.25$. $\Sigma_{br,m} = 1.22e-5\mathbf{I}_{2\times2}$. The measurement noise covariance in KF and UKF is set as $\mathbf{R} = \mathrm{diag}(1.22e-51.22e-52.25)$.

Two simulation experiments will be carried out with two types of IMU.

Simulation 1: test with the MEMS IMU

The position errors of different methods using MEMS IMU are compared in Fig. 5.

According to sensor error parameters of MEMS IMU, the initial pre-integration covariance in FGO is set as $\mathbf{Q} =$

Authorized licensed use limited to: Hong Kong Polytechnic University. Downloaded on July 13,2023 at 10:26:38 UTC from IEEE Xplore. Restrictions apply.

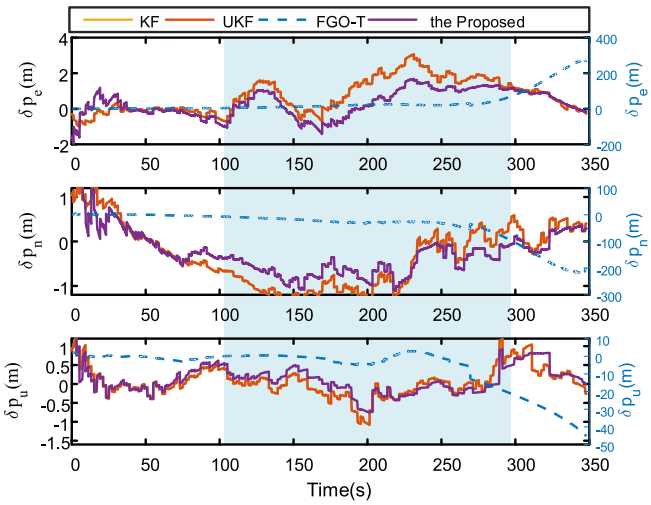

Fig. 6. Comparison of the position estimation error using FOG IMU.

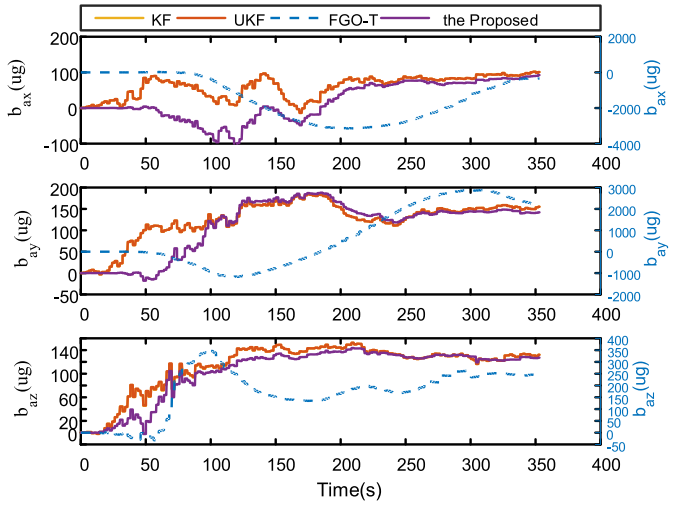

Fig. 7. Estimation result of accelerometer bias.

$\mathrm{diag}[3.4e-9\mathbf{I}_{1\times3}, 1.1e-5\mathbf{I}_{1\times3}]$. The process noise covariance in KF and UKF is set as $\mathbf{Q} = \mathrm{diag}(3.4e-9\mathbf{I}_{1\times3}, 1.1e-5\mathbf{I}_{1\times3})$.

It can be seen from Fig. 5 that the performance of the three methods is similar in the case of MEMS IMU. Simulation 1 is conducted to prove that the traditional IMU pre-integration model is appropriate and is suitable for the positioning scenarios in the field of robotics with MEMS IMU.

Simulation 2: test with the FOG IMU

Simulation 2 is conducted to prove that the traditional pre-integration model is not appropriate in the case of high precision IMU and the proposed method is the best of all.

According to sensor error parameters of FOG IMU, the initial pre-integration covariance in FGO is set as $\mathbf{Q} = \mathrm{diag}[8.5e-12\mathbf{I}_{1\times3}, 9.56e-7\mathbf{I}_{1\times3}]$. The process noise covariance in KF and UKF is set as $\mathbf{Q} = \mathrm{diag}(8.5e-12\mathbf{I}_{1\times3}, 9.56e-7\mathbf{I}_{1\times3})$.

The position errors in the stable phase of the navigation process using FOG IMU are compared in Fig. 6.

It can be seen from Fig. 6 that the position error of the FGO-T method diverges due to the inaccurate IMU integration model. The right y-axis is corresponding to the errors of FGO-T. It has a maximum error of about 300m. Thus, the traditional IMU integration model is not suitable for the underwater fiber optics inertial navigation system.

The positioning accuracy of KF is similar to that of UKF. The proposed method performs better than KF and UKF in the stable phase of the navigation process. Take the blue area in the figure as an example. The error of the proposed method is closer to zero.

The bias factor is also involved in the factor graph as Fig. 3 shows. Thus, the bias estimation results are shown in Figs. 7 and 8.

In Fig. 7, the accelerometer bias of the proposed method is similar to that of the KF and UKF methods. The accelerometer bias can be well estimated through the three methods. However, the bias estimation accuracy of the traditional IMU pre-integration model is lower than the proposed method. It doesn't even converge near the truth value.

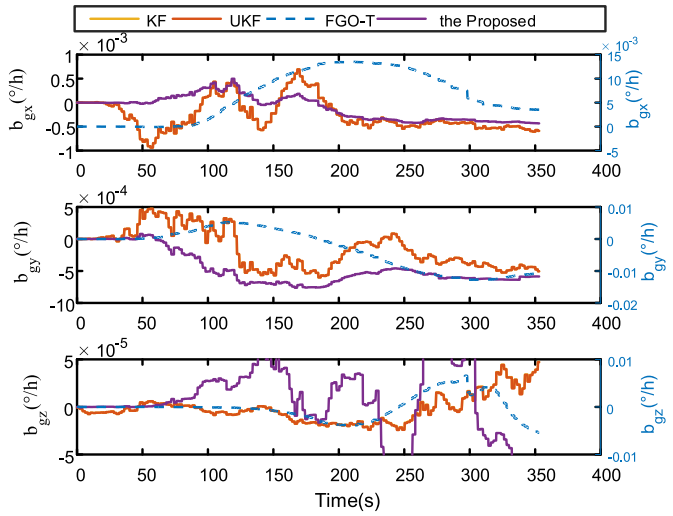

Fig. 8. Estimation result of gyroscope bias.

In Fig. 8, it can be seen that as the observability of the gyroscope bias is very weak, it is difficult to estimate the bias through these methods.

To analyze the position error quantitatively, the root-mean-square error (RMSE), the Average Location Error (ALE), and the Average Horizontal Error (AHE) are used as the performance metrics. The AHE and ALE are defined as follows.

$$ALE = \frac{1}{n}\sum_{k=1}^{n}\sqrt{(\tilde{x}_k - x_k)^2 + (\tilde{y}_k - y_k)^2 + (\tilde{z}_k - z_k)^2}$$

$$AHE = \frac{1}{n}\sum_{k=1}^{n}\sqrt{(\tilde{x}_k - x_k)^2 + (\tilde{y}_k - y_k)^2} \tag{41}$$

where $\tilde{x}_k$ is the estimated value at epoch k and x_k is the true value. The same definition is used for y and z. The statistical results are shown in Table II.

It can be seen from Table II that the proposed method exhibits a better performance than KF and UKF in both AHE and ALE. The FGO with the traditional pre-integration model performs worst. The errors in the simulation were random errors. Thus,

Authorized licensed use limited to: Hong Kong Polytechnic University. Downloaded on July 13,2023 at 10:26:38 UTC from IEEE Xplore. Restrictions apply.

TABLE II
RMSE COMPARISON OF THE DIFFERENT METHODS

	EPE(m)	NPE(m)	UPE(m)	AHE(m)	ALE(m)
KF	1.25	0.72	0.38	1.26	1.32
UKF	1.25	0.72	0.38	1.26	1.32
FGO-T	80.57	78.09	14.66	67.97	68.63
The Proposed	**0.82**	**0.50**	**0.36**	**0.88**	**0.95**

NPE, EPE, and UPE denote the RMSE of the north potion, east position, and up position.

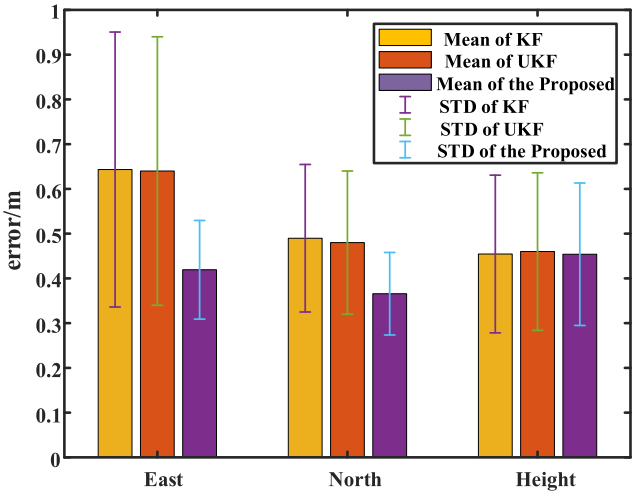

Fig. 9. Comparison of the position estimation error in Monte Carlo simulation.

an individual experiment may be accidental. To make the results more convincing, we conducted statistics on the results of 20 independent experiments. The mean and standard deviation (STD) of the Monte Carlo simulation test is used as the performance metric. It is defined as follows.

$$\mathrm{E}_{x,k} = \sqrt{1/M \sum_{s=1}^{M} (x_k^s - \tilde{x}_k^s)^2}$$

$$\mathrm{Mean}_x = \frac{1}{N} \sum_{k=1}^{N} \mathrm{E}_{x,k}$$

$$\mathrm{STD}_x = \sqrt{\frac{1}{N-1} \sum_{k=1}^{N} |\mathrm{E}_{x,k} - \mathrm{Mean}_x|^2} \tag{42}$$

where $M = 20$, $\tilde{x}_k^s$ is the estimated value at s-th Monte Carlo run at epoch k and x_k^s is the true value. The same definition is used for y and z. N is the length of the data.

The error of the FGO-T method is too large to be comparable. Thus, only the KF, UKF, and the proposed method are compared below. The error bar is shown in Fig. 9.

It can be seen from Fig. 9. that the accuracy of the proposed method is improved obviously in the horizontal direction. Both mean and STD are better than KF and UKF methods.

Simulations 1 and 2 proved that the traditional pre-integration model is only suitable for the low-cost IMU. In FOG applications, the errors could be very large. With the improved IMU pre-integration model, the FGO can show better performance than KF and UKF for the INS/USBL integrated navigation system.

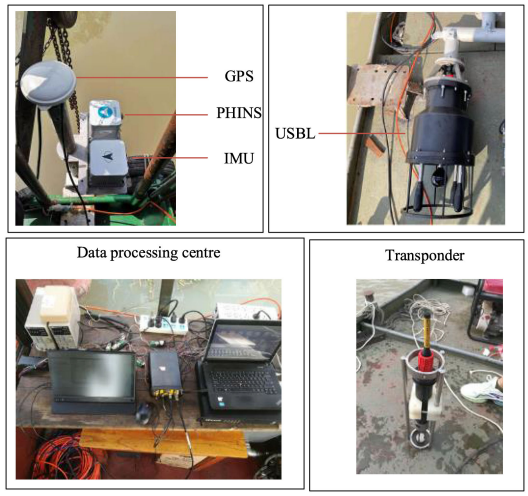

Fig. 10. Diagram of the experimental scene.

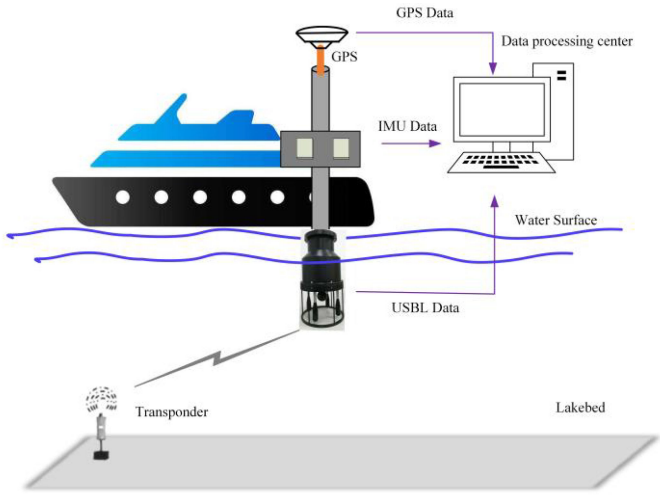

Fig. 11. Description of the experimental scene.

B. Field Test

In addition to the simulation experiments, we also carried out field tests on the Yangtze River in Jiangsu Province, China. The experimental scene and sensors involved in the experiment are shown in Fig. 10.

In Fig. 10, the transponder is placed at the bottom of the river. The USBL is mounted on the side of the ship and placed below the surface of the water. The data processing center is responsible for receiving USBL and IMU data and processing navigation results, as Fig. 11 shows. The position of PHINS/GPS integrated system is used as the ground truth.

The performance of the sensors is as follows.

a) Inertial measurement unit

Gyro:

constant drift $\leq 0.01^\circ/h$, stochastic drift $\leq 0.005^\circ/\sqrt{h}$;

constant drift repeatability $\leq 0.01^\circ/h$;

Authorized licensed use limited to: Hong Kong Polytechnic University. Downloaded on July 13,2023 at 10:26:38 UTC from IEEE Xplore. Restrictions apply.

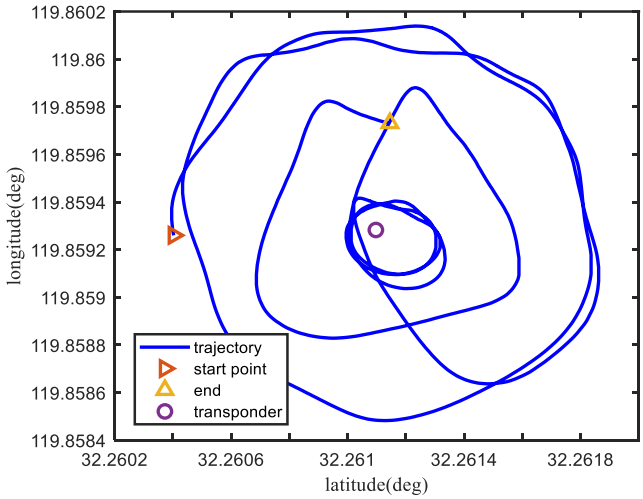

Fig. 12. Experiment trajectory.

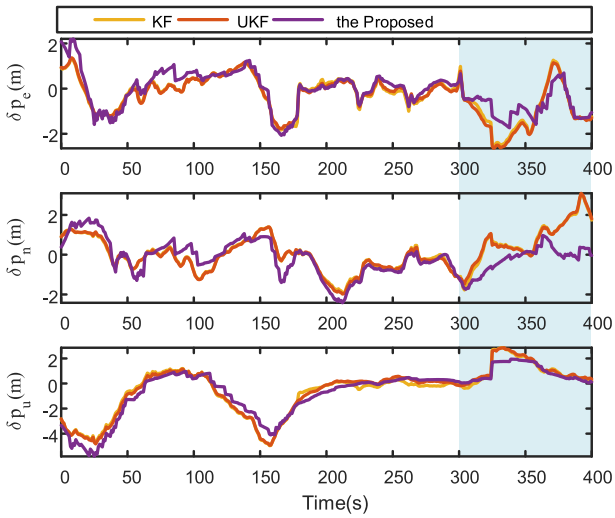

Fig. 13. Comparison of the position error in the field test.

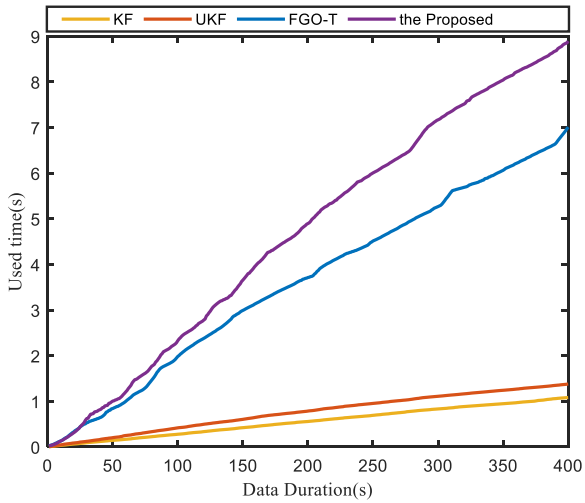

Fig. 14. The comparison of the execution time.

scale factor repeatability $\leq$ 50ppm(1σ);
Output frequency: 200 Hz.
Accelerometer:
bias $\leq$100μg, random walk $50ug/\sqrt{Hz}$;
scale factor repeatability $\leq$ 35ppm(1σ); full scale $\pm$20g;
b) USBL
Positioning error: 0.1m+1%r;
Output frequency: 1/2 Hz.
c) PHINS/GPS integrated system
positioning accuracy aided by RTK GPS: 0.02-0.05m;
accuracy of yaw: 0.01 $^\circ/cosL$;

The covariance of USBL in FGO is set as $\Sigma_{sl,m} = 6.\ \Sigma_{br,m} = 0.0037\mathbf{I}_{2\times2}$. The measurement noise covariance in KF and UKF is set as $\mathbf{R} = \text{diag}(0.0037, 0.0037, 6)$.

The initial pre-integration covariance in FGO is set as $\mathbf{Q} = \text{diag}[2.1e-12\mathbf{I}_{1\times3}, 9.57e-7\mathbf{I}_{1\times3}]$. The process noise covariance in KF and UKF is set as $\mathbf{Q} = \text{diag}(2.1e-12\mathbf{I}_{1\times3}, 9.57e-7\mathbf{I}_{1\times3}, 0_{1\times9})$.

The installation angle between USBL and INS and the transponder position are calibrated in advance, which can be seen in our previous work [10].

The vehicle is sailing on the surface of the river and the velocity is about 3 m/s. The trajectory in the experiment is shown in Fig. 12.

As the FGO-T is not suitable for underwater fiber-optic inertial navigation, the KF, UKF, and the proposed method are selected for comparison. The position error is shown in Fig. 13.

It can be seen from Fig. 13 that the proposed method outperforms the KF and UKF methods in the stable phase of navigation. Especially at the end of the navigation process, the position error of the proposed method is more stable and closer to zero than the KF and UKF methods. As the blue area is shown in Fig. 13. To analyze the position error quantitatively, the RMSE, ALE, and AHE are used as performance metrics. The statistical results in the stable phase of navigation (50s-400s) are shown in Table III

In Table III, the proposed method exhibits a better performance than KF and UKF in both AHE and ALE. The position accuracy is improved by 15.67%, 13.94%, and 16.65% respectively compared with the KF method in terms of EPE, NPE, and UPE.

TABLE III
RMSE COMPARISON OF DIFFERENT METHODS IN FIELD TEST

	EPE(m)	NPE(m)	UPE(m)	AHE(m)	ALE(m)
KF	0.92	0.95	1.56	1.12	1.69
UKF	0.93	0.95	1.55	1.13	1.69
The Proposed	**0.78**	**0.82**	**1.30**	**0.99**	**1.48**

The INS/USBL integration is a nonlinear system. The superiority of FGO is attributable to the multiple iterations and re-linearization and greater amount of data applied in the FGO. The application of multiple iterations and re-linearization solves the problem of nonlinearity and improves the precision of the INS/USBL integrated navigation system. Thus, the simulation and field test confirmed the potential of the application of factor graph in underwater high precision navigation and positioning.

Authorized licensed use limited to: Hong Kong Polytechnic University. Downloaded on July 13,2023 at 10:26:38 UTC from IEEE Xplore. Restrictions apply.

C. Discussion of the Computational Load

A problem faced in FGO applications is the computational load. Execution time of different algorithms can represent the computational load [23], [24]. To analyze the computational load of different algorithms, a comparison of the execution time among different algorithms is given in Fig. 14.

In Fig. 14, the vertical coordinate expresses the run time of the program while the horizontal coordinate is the duration of data. As only the current state is estimated, the execution times of the Kalman filter-based method are less than the FGO-based method. The application of multiple iterations and greater amount of data make the FGO method suffer from a huge computational load. The proposed IMU pre-integration model is more complex than the traditional pre-integration model as the earth rotation is considered. Its execution time is larger than that of the traditional FGO method. Although the FGO method needs more computational load, it is an alternative method when computer performance is sufficient.

VI. Conclusion

This paper proposes a novel integrated navigation scheme for underwater INS/USBL integration system via factor graph. Different from the existing Kalman filter scheme, the FGO utilizes a large amount of data in the sliding window to improve the estimation accuracy. In addition, multiple iterations and re-linearization of FGO can also solve the nonlinear problem of USBL measurements. To make FGO suitable for a high-precision inertial navigation system, an IMU pre-integration model considering the earth rotation is proposed. The simulation and field test showed that the traditional pre-integration model can not meet the requirements of underwater applications and will cause great position errors. The proposed method plays better performance than the traditional FGO and KF method. It exhibits great potential for underwater navigation applications.

This paper shows the feasibility of applying FGO to integrated navigation of underwater FOG inertial navigation systems. In future research, a more accurate pre-integration model needs to be further studied if a higher precision IMU is adapted. Considering the complex underwater environment, the robust FGO method also needs to be researched in the presence of outliers. FGO will become a new key technology for underwater navigation.

References

[1] B. Wang, J. Zhu, Z. Deng, and M. Fu, "A characteristic parameter matching algorithm for gravity-aided navigation of underwater vehicles," *IEEE Trans. Ind. Electron.*, vol. 66, no. 2, pp. 1203–1212, Feb. 2019.

[2] Y. Yao, X. Xu, D. Yang, and X. Xu, "An IMM-UKF aided SINS/USBL calibration solution for underwater vehicles," *IEEE Trans. Veh. Technol.*, vol. 69, no. 4, pp. 3740–3747, Apr. 2020.

[3] L. Zhang, T. Zhang, H. -S. Shin, and X. Xu, "Efficient underwater acoustical localization method based on time difference and bearing measurements," *IEEE Trans. Instrum. Meas.*, vol. 70, 2021, Art. no. 8501316.

[4] B. Wang, Q. Ren, Z. Deng, and M. Fu, "A self-calibration method for nonorthogonal angles between gimbals of rotational inertial navigation system," *IEEE Trans. Ind. Electron.*, vol. 62, no. 4, pp. 2353–2362, Apr. 2015.

[5] L. Zhang and T. Zhang, "A fast calibration method for dynamic lever-arm parameters for IMUs based on the backtracking scheme," *IEEE Trans. Instrum. Meas.*, vol. 69, no. 9, pp. 6946–6956, Sep. 2020.

[6] M. Morgado, P. Oliveira, C. Silvestre, and J. F. Vasconcelos, "USBL/INS tightly-coupled integration technique for underwater vehicles," in *Proc. 9th Int. Conf. Inf. Fusion*, Jul. 2006, pp. 1–8.

[7] M. Morgado, P. Oliveira, and C. Silvestre, "Tightly coupled ultrashort baseline and inertial navigation system for underwater vehicles: An experimental validation," *J. Field Robot.*, vol. 30, no. 1, pp. 142–170, Jan. 2013.

[8] Y. Zhang, M. Mo, X. Ma, and J. Deng, "An algorithm used in underwater SINS /USBL integrated navigation," *Navigation Positioning Timing*, vol. 3, no. 2, pp. 7–13, 2016.

[9] P. Dong, J. Cheng, L. Liu, and H. Mou, "INS/USBL nonlinear integrated navigation method based on observations of relative information," *Syst. Eng. Electron.*, vol. 41, no. 2, pp. 402–408, 2019.

[10] T. Zhang, L. Zhang, and H. -S. Shin, "A novel and robust calibration method for the underwater transponder position," *IEEE Trans. Instrum. Meas.*, vol. 70, 2021, Art. no. 9500512.

[11] B. Xu *et al.*, "A novel robust filter for outliers and time-varying delay on an SINS/USBL integrated navigation model," *Meas. Sci. Technol.*, vol. 32, no. 1, 2021, Art. no. 015903.

[12] B. Xu, X. Wang, J. Zhang, and A. A. Razzaqi, "Maximum correntropy delay Kalman filter for SINS/USBL integrated navigation," *ISA Trans.*, vol. 117, pp. 274–287, 2021.

[13] J. Wang, T. Zhang, B. Jin, Y. Zhu, and J. Tong, "Student's t-Based robust Kalman filter for a SINS/USBL integration navigation strategy," *IEEE Sensors J.*, vol. 20, no. 10, pp. 5540–5553, May 2020.

[14] T. Zhang, J. Wang, L. Zhang, and L. Guo, "A student's T-Based measurement uncertainty filter for SINS/USBL tightly integration navigation system," *IEEE Trans. Veh. Technol.*, vol. 70, no. 9, pp. 8627–8638, Sep. 2021.

[15] T. Qin, P. Li, and S. Shen, "VINS-Mono: A robust and versatile monocular visual-inertial state estimator," *IEEE Trans. Robot.*, vol. 34, no. 4, pp. 1004–1020, Aug. 2018, doi: 10.1109/TRO.2018.2853729.

[16] T. Shan, B. Englot, D. Meyers, W. Wang, C. Ratti, and D. Rus, "LIO-SAM: Tightly-coupled lidar inertial odometry via smoothing and mapping," in *Proc. IEEE/RSJ Int. Conf. Intell. Robots Syst.*, 2020, pp. 5135–5142.

[17] N. Sünderhauf and P. Protzel, "Towards robust graphical models for GNSS-based localization in urban environments," in *Proc. Int. Multi-Conf. Syst., Signals Devices*, 2012, pp. 1–6.

[18] X. Bai, W. Wen, and L. -T. Hsu, "Time-correlated window Carrier-phase aided GNSS positioning using factor graph optimization for urban positioning," *IEEE Trans. Aerosp. Electron. Syst.*, vol. 58, no. 4, pp. 3370–3384, Aug. 2022.

[19] W. Wen, G. Zhang, and L. -T. Hsu, "GNSS outlier mitigation via graduated non-convexity factor graph optimization," *IEEE Trans. Veh. Technol.*, vol. 71, no. 1, pp. 297–310, Jan. 2022.

[20] C. Forster, L. Carlone, F. Dellaert, and D. Scaramuzza, "On-Manifold preintegration for real-time visual–inertial odometry," *IEEE Trans. Robot.*, vol. 33, no. 1, pp. 1–21, Feb. 2017.

[21] S. Bai, J. Lai, P. Lyu, Y. Cen, and B. Ji, "Improved preintegration method for GNSS/IMU/In-Vehicle sensors navigation using graph optimization," *IEEE Trans. Veh. Technol.*, vol. 70, no. 11, pp. 11446–11457, Nov. 2021.

[22] Q. Li, L. Zhang, and X. Wang, "Loosely coupled GNSS/INS integration based on factor graph and aided by ARIMA model," *IEEE Sensors J.*, vol. 21, no. 21, pp. 24379–24387, Nov. 2021.

[23] S. Bai, J. Lai, P. Lyu, B. Ji, B. Wang, and X. Sun, "A novel plug-and-play factor graph method for asynchronous absolute/relative measurements fusion in multi-sensor positioning," *IEEE Trans. Ind. Electron.*, vol. 70, no. 1, pp. 940–950, Jan. 2023.

[24] W. Wen, T. Pfeifer, X. Bai, and L.-T. Hsu, "Factor graph optimization for GNSS/INS integration: A comparison with the extended Kalman filter," *Navigation*, vol. 68, no. 2, pp. 315–331, 2021.

[25] V. Indelman, S. Williams, M. Kaess, and F. Dellaert, "Factor graph based incremental smoothing in inertial navigation systems," in *Proc. 15th Int. Conf. Inf. Fusion*, Singapore, 2012, pp. 2154–2161.

[26] S. Agarwal and K. Mierle, and Others, "Ceres solver," [Online]. Available: http://ceres-solver.org

[27] X. He, Y. Le, and W. Xiao, "MEMS IMU and two-antenna GPS integration navigation system using interval adaptive Kalman filter," *IEEE Aerosp. Electron. Syst. Mag.*, vol. 28, no. 10, pp. 22–28, Oct. 2013.

[28] K. H. Kim, J. G. Lee, and C. G. Park, "Adaptive two-stage extended Kalman filter for a fault-tolerant INS-GPS loosely coupled system," *IEEE Trans. Aerosp. Electron. Syst.*, vol. 45, no. 1, pp. 125–137, Jan. 2009.

Authorized licensed use limited to: Hong Kong Polytechnic University. Downloaded on July 13,2023 at 10:26:38 UTC from IEEE Xplore. Restrictions apply.

[29] H. Xiong, R. Bian, Y. Li, Z. Du, and Z. Mai, "Fault-tolerant GNSS/SINS/DVL/CNS integrated navigation and positioning mechanism based on adaptive information sharing factors," *IEEE Syst. J.*, vol. 14, no. 3, pp. 3744–3754, Sep. 2020.
[30] H. Tang, X. Niu, T. Zhang, J. Fan, and J. Liu, "Exploring the accuracy potential of IMU preintegration in factor graph optimization," Sep. 2021, Accessed: Sep. 8, 2021. [Online]. Available: https://arxiv.org/abs/2109.03010v1
[31] S. Liu, T. Zhang, and L. Zhang, "A SINS aided correct method for USBL range based on maximum correntropy criterion adaptive filter," *IEEE Trans. Instrum. Meas.*, vol. 71, 2022, Art. no. 8501913.

Liang Zhang received the Ph.D. degree in instruments science and technology from Southeast University, Nanjing, China, in 2021, and the M.S. degree in navigation, guidance, and control from the Nanjing University of Aeronautics and Astronautics, Nanjing, China, in 2017. He is currently a Postdoctoral Fellow with the Interdisciplinary Division of Aeronautical and Aviation Engineering, Hong Kong Polytechnic University. His research interests include inertial navigation, integrated navigation technology, and underwater positioning technology.

Li-Ta Hsu received the B.S. and Ph.D. degrees in aeronautics and astronautics from National Cheng Kung University, Tainan City, Taiwan, in 2007 and 2013, respectively. He is currently an Associate Professor with the Department of Aeronautical and Aviation Engineering, The Hong Kong Polytechnic University. He is also Limin Endowed Young Scholar in Aerospace Navigation. He was a Visiting Researcher with the Faculty of Engineering, University College London, London, U.K., and the Tokyo University of Marine Science and Technology, Tokyo, Japan, in 2012 and 2013, respectively. Dr. Hsu was selected as a Japan Society for the Promotion of Sciences Postdoctoral Fellow with the Institute of Industrial Science, University of Tokyo, Tokyo, Japan, and worked from 2014 to 2016. He is an Associate Fellow with the Royal Institute of Navigation, London, U.K. He is currently a member of ION and and a member of the editorial board and reviewer in professional journals related to GNSS. In 2013, he won a Student Paper Award and two Best Presentation Awards from the Institute of Navigation (ION).

Tao Zhang received the Ph.D. degree in precision instrument and machinery from Southeast University, Nanjing, China, in 2008. He is currently a Professor with the School of Instrument Science and Engineering, Southeast University. His research interests include inertial navigation, AUV underwater positioning, and integrated navigation.

Authorized licensed use limited to: Hong Kong Polytechnic University. Downloaded on July 13,2023 at 10:26:38 UTC from IEEE Xplore. Restrictions apply.